Charge Fractionalization in Quantum Wires

Permanent link

Terms of Use

Share Your Story

Charge Fractionalization in Quantum Wires

Hadar Steinberg[1], Gilad Barak[1], Amir Yacoby[1,2], Loren N. Pfeiffer[3], Ken W. West[3], Bertrand I. Halperin[2], Karyn Le Hur[4]

[1]*Department of Condensed Matter Physics, Weizmann Institute of Science, Rehovot 76100, Israel.*

[2]*Department of Physics, Harvard University, Cambridge MA, 02138, USA.*

[3]*Bell Labs, Lucent Technologies, 700 Mountain Avenue, Murray Hill, NJ 07974, USA.*

[4]*Department of Physics, Yale University, New Haven, CT 06520, USA.*

The unit of charge in nature is a fundamental constant. In reduced dimension, however, charge may be fractionalized. A prominent example in two dimensions is the fractional quantum Hall effect in which the elementary charge excitations are quantized to $e/(2p+1)$, where e is the unit of electric charge and p is an integer[1-3]. Quantum one-dimensional (1D) systems have also been theoretically predicted to carry charge in units smaller than a single electron charge. Unlike 2D systems, the charge excitations in 1D are not quantized and depend directly on the strength of the Coulomb interactions. For example, in a system with momentum conservation, it is predicted that the charge of a unidirectional electron that is injected into the wire decomposes into a right and left moving charge excitations carrying fractional charge $f_0 e$ and $(1-f_0)e$ respectively[4,5]. f_0 approaches unity for non-interacting electrons and is less than one for repulsive interactions. In this work we provide the first direct measurements of fractional charge in 1D. We realize a 3-terminal geometry where unidirectional electrons are injected at the bulk of a wire and the resulting current at drains located on both sides is measured. The result is presented in terms of an asymmetry parameter, defined as $AS = (I_R-I_L)/(I_R+I_L)$, $I_{R,L}$ being the currents detected on the right and left. AS depends on the extent of fractionalization, but also on details of the coupling at the drains. We evaluate the effect of drain coupling by measuring the 2-terminal conductance G_{2T} between the right and left drains, finding that $G_{2T}/G_0 = AS$, where $G_0 = (2e^2/h)$ is the quantum of

conductance. We argue, based on a theoretical model that this observed equality proves that the tunneling electron charge fractionalizes as predicted by theory.

Charge fractionalization in 1D is already predicted for the spinless Luttinger model[4,5]. The charge fraction f_0 is given by

$$f_0 = (1 + g_c)/2, \tag{1}$$

where g_c is the Luttinger liquid interaction parameter. For a Galilean invariant system, $g_c = v_F/v_c$, where v_F is the bare Fermi velocity and v_c is the velocity of charge excitations. Roughly, $g_c \approx (1 + U/2\varepsilon_F)^{-1/2}$, where U is the Coulomb interaction energy, and ε_F is the Fermi energy. In a spinful 1D system, this charge fractionalization occurs in addition to spin-charge separation, which is another type of electron fractionalization. Spin-charge separation has been recently confirmed by spectroscopy and tunneling experiments[6-8] and will therefore not be addressed in this work.

Observing charge fractionalization in an experiment is a considerable challenge: In 2D, Laughlin's theory of the fractional quantum Hall effect was confirmed by low-frequency shot-noise measurements[1,3], as well as by direct charge sensing with a single electron transistor[9]. However, FQH edge states are *chiral*, propagating along the edges of a 2-Dimensional Electron Gas (2DEG), so that counter-propagating modes are spatially separated. In contrast, the *non-chiral* quantum wire modes are confined to the same spatial channel, and cannot be contacted individually. As a result their chemical potentials renormalize in a non-trivial manner when adiabatically coupled to metallic leads, making interaction physics difficult to observe. For example, the DC 2-terminal conductance with ideal contacts is universal and given by $G = G_0 \equiv 2e^2/h$, independent of interactions[5,10-13]. Furthermore, low-frequency shot-noise measurements in an ideal wire would only reveal the physics of the Fermi-liquid contacts, remaining insensitive to fractionalization[14]. Although this difficulty is removed at frequencies exceeding $v_F / g_c L \sim 10^{10}$ *Hz*, where the excitation wave-length is shorter than the wire segment[15-17], these frequencies are difficult to explore experimentally at low-temperatures.

Initial experimental indication of electron fractionalization in 1D is provided by angle-resolved photo-emission spectroscopy (ARPES) measurements on stripe-ordered cuprate

2

materials[8]. Recent theoretical studies have proposed transport experiments aimed at detecting the same physics in quantum wires. Generally, these involve the realization of multi-terminal geometries, including: (i) Local injection of electrons into a wire, where high-frequency noise-correlations are expected[15]; (ii) A four-probe geometry, measuring voltage shot-noise due to an impurity[18]; (iii) Studying the DC *I(V)* curves in the presence of a bulk contact[19]; (iv) Measuring the suppression of Aharonov-Bohm interference between two weakly coupled wires [20].

In this work we realize our own version of a multi-terminal geometry: We use a double-wire system previously applied to the study of spin-charge separation[7,21] and localization in 1D[22]. Using momentum conservation in the tunneling process between the two wires we inject unidirectional electrons to the bulk of a wire, with fractionalization resulting in currents detected on both sides of the injection region. The ratio of these currents together with a 2-terminal reference measurement and a separate measurement of g_c allows us to extract the extent of charge fractionalization.

The double quantum-wire sample (Figure 1a) is prepared using Cleaved Edge Overgrowth (CEO): Two parallel 2D quantum wells are grown by standard techniques in a GaAs / AlGaAs heterostructure, followed by cleavage in the MBE vacuum chamber and a subsequent growth sequence on the cleaved plane. The second growth-sequence induces 1D channels that are quantum confined at the edge of the quantum wells. The Upper Wire (UW) is 20 nm or 25 nm wide, and the Lower Wire (LW) is 30 nm wide. They are separated by a 6 nm wide barrier, 300 mV high, designed to allow measurable tunneling.

The samples are designed to have only the top 2DEG populated (light blue in Figure 1a), serving as a contact to the UW (dark blue) at its edge. The experimental geometry is controlled by the application of negative voltage to tungsten top-gates. The gates are tuned to deplete the UW while leaving the LW (dark green) continuous. The 3-terminal geometry which is presented in the figure requires biasing two gates (G_1 and G_2) defining a finite central junction of length $L_S = 10\text{-}40 \ \mu m$, and a semi-infinite junction on each side. The short junction serves as the source and the long junctions 1 and 3 as drains. We measure the differential tunneling conductance $\partial I_T / \partial V_{SD}$ between the source and each

drain using standard lock-in techniques. Typically dV_{SD} is 14 μV and the frequency a few Hz. The measurements are performed in a ^{3}He refrigerator at $T = 0.25 \ K$.

Since $L_S \gg 1/k_F$, and the wires are parallel to within atomic precision, even the finite source junction is in effect translationally invariant and the tunneling electrons conserve both energy ε and momentum $\hbar k$, k being the wave-number. Source-drain voltage V_{SD} controls the energy of the tunneling electrons. Here the DC component of V_{SD} is set to zero, and an AC component, smaller than temperature, is added for lock-in purposes. A magnetic field, B, applied perpendicular to the cleave plane, adds momentum $\hbar q_{\mathbf{B}} = eBd$ to the tunneling electrons, d being the distance between the centers of the wires. It is instructive to describe tunneling between the wires in terms of their energy-momentum dispersions. B has the effect of shifting both dispersions relative to one another along the momentum axis, as seen in the Fig. 2a, which depicts their relative positions for various magnetic fields. Since $V_{SD} = 0$, both dispersions have the same electro-chemical potential. The UW is represented by the dispersions of one 1D mode and the 2DEG, and the LW by one 1D mode. The dispersions are presented by parabolae as an illustration, but in reality are more complex due to electron-electron interactions. Typically at $B = 0$ the two 1D dispersions do not overlap (i), since the wires have different densities, and tunneling is suppressed. Applying a field B^- shifts the dispersions to overlap near one of the Fermi-points (ii), allowing tunneling between co-propagating electrons. The high field crossing of the two dispersions, where electrons tunnel between counter-propagating modes is marked as B^+ (iv, v) where $B^{\pm} = \hbar \left| k_F^U \pm k_F^L \right|$, U/L standing for UW / LW. A key feature of this measurement geometry is that at $B = B^{\pm}$, electrons with a well-defined momentum-state, near the Fermi-point, are added to the LW. Typically each wire is populated by several sub-bands, but tunneling between different sub-bands is suppressed by near-orthogonality [21], so that each sub-band j contributes a single pair of peaks, denoted $B_j^{\pm}$.

In Figure 2b the right and left differential conductances $\partial I_R/\partial V_{SD}$ and $\partial I_L/\partial V_{SD}$ for $L_S = 10$ μm are plotted vs. B. They are measured by applying differential voltage at the source, and reading the current at each of the left and right drains. As B is scanned from zero to positive fields, small, sharp peaks are first encountered at $B^-_{1,2}$. The wide feature at 1T<B<3T results from tunneling between the populated 2DEG in the upper quantum well and the LW (Fig 2a (iii)). Further increasing the field, we finally encounter the B^+ feature

4

at $B = 6.5T$. In order to check whether the original directionality of the injected electrons is conserved, we now compare the conductance of both drains. Pronounced directional asymmetry emerges near the B^+ feature: At $B = +B^+$ left-moving electrons are injected into the LW (Fig 2a (iv)), and the current detected at the left drain is indeed significantly stronger than on the right. Exactly opposite values appear at $B = -B^+$, attesting to the geometric symmetry of the sample. A similar effect appears near the B^- features, but is more difficult to observe since the differential conductance is small relative to a strong background signal. We note that the current associated with injection from the 2DEG is relatively symmetric. This suggests that the 2D-1D tunneling conductance may involve significant contribution from processes which do not conserve momentum.

The effect observed near $-B^+$ is quantified by an asymmetry parameter $AS \equiv (I_R - I_L)/(I_R + I_L)$; The deviation from perfect asymmetry cannot a-priori be attributed to fractionalization since the wire is not perfect, and microscopic effects such as back-scattering can suppress AS by distributing the charge evenly in the wire before it has chance to be detected. Moreover, complicated processes associated with coupling of the interacting wire with the non-interacting leads also take place in the drains and may lead to a smaller overall asymmetry. In order to isolate fractionalization physics from such microscopic effects we also measure the 2-terminal conductance between the left and right drains. The 2-terminal conductance, being independently sensitive to these microscopic processes, allows us to extract the extent of fractionalization from AS. To demonstrate this we use a model (the geometry of which is depicted in figure 1b) derivable from Luttinger liquid theory when a single sub-band is occupied in the LW. The model should also be a good approximation when there are several occupied sub-bands, as the contacts communicate with only one of the sub-bands, scattering between sub-bands is small, and gates $G_{1,2}$ transmit only the lowest sub-band.

The chemical potentials $V_{1,3}$ in the UW (subscript indicates junction) are set by the 2DEG that couples to both right and left-moving UW modes [23]. According to Luttinger liquid theory, we may define separate chemical potentials for right and left-moving LW charge modes on each side of the central junction, denoted $y_{1,3}$, $w_{1,3}$ respectively. These are defined so that the current (right-moving) at any point is given by $I = g_c G_0 (y - w)$, where $G_0 = 2e^2/h$, while $w+y$ is determined by the charge density, such that in equilibrium,

where $I=0$, y and w are equal to the electron chemical potential V. With these definitions, one finds that a right moving charge excitation will affect the local value of y, but leave w unchanged, and vice versa. At the two end contacts, if the currents are small enough so that linear response applies, we must have $y_1 = \beta V_1 + \gamma w_1$, $w_3 = \beta V_3 + \gamma y_3$, where the parameters β and γ must satisfy $\beta + \gamma = 1$ so that $y=w=V$ in equilibrium. We have assumed here that the two junctions have identical parameters. We note without limiting the generality of the model, β accounts for both backscattering occurring in the LW as well as any process associated with the coupling of the LW to the Fermi liquid leads.

For the two-terminal conductance, no current enters the LW at the center contact, so if there is no scattering there, we must have $w_1 = w_3$ and $y_1 = y_3$, and we compute $G_{2T} = I/(V_3 - V_1)$. This yields $G_{2T} = g_c G_0 \beta/(2 - \beta)$. We note that the g_c dependence is a consequence of the boundary conditions at equilibrium. For the three terminal conductance, we set $V_1 = V_3 = 0$, and require that $I_R + I_L = I_S$, where I_S is the injected current, $I_R = g_c G_0 (y_3 - w_3)$ is the net right-moving current in the right half of the wire and $I_L = g_c G_0 (w_1 - y_1)$ is the left-moving current in the left half of the wire .

At $B = -B^+$, where the center contact injects right moving electrons, if we assume that an (unknown) fraction f of each electron charge travels to the right, this means that $g_c G_0 (y_3 - y_1) = I_S f$ and $g_c G_0 (w_1 - w_3) = I_S (1-f)$.

Now solving for $AS = (I_R - I_L)/(I_R + I_L)$ we obtain:

$$AS = \frac{\beta}{2 - \beta}(2f - 1),\tag{2}$$

and hence the ratio:

$$\frac{G_{2T}[G_0]}{AS} = \frac{g_c}{2f - 1},(\textbf{Error!} \quad \textbf{Bookmark} \quad \textbf{not}$$

defined.3)

at least for a single mode wire. This is a fundamental result: It implies that regardless of the microscopic details, it is sufficient to measure G_{2T} , AS and g_c under the same conditions in order to extract f.

We therefore proceed to measure G_{2T} between contacts O_1 and O_3, (Figure 1a). This requires tuning the voltage of a single gate (G_2 or G_1 in the figure) to deplete the UW. Since coupling to the LW is via tunneling, G_{2T} depends on B, and should be maximal

when $B = B^+$. G_{2T} vs. V_G scans are presented in Figure 3a, depicting line-scans taken at different magnetic fields close to B^+. For $V_G = -1.58$ V conductance through the UW is suppressed. For $-1.76 < V_G < -1.58$ V current flows through the LW, coupled by junctions 1, 3. For each line-scan $G_{2T}(B)$ is taken as the maximal value in this range and is presented as a dot in panel B. The result appears to fit a Lorentzian, possibly related to variations of the density or of the tunneling rate along the wire.

We study the ratio G_{2T} / AS by comparing $G_{2T}(B^+)$ and $AS(B^+)$ at different wire densities. Density is controlled either by biasing a side-gate, evaporated over the cleave plane, or by shining infrared light on the sample. The results are plotted in Figure 4. In the observed density-range G_{2T} appears to depend linearly on n_L, the line intercepting $G_{2T}(n_L) = 0$ at a finite density of $n_L = 20$ μm^{-1}. The mechanism underlying this dependence is not understood. Superimposing the asymmetry results on this plot yields the key experimental finding of this work: $AS(n_L)$ lies on top of the $G_{2T}(n_L)$ line, showing that $G_{2T} = AS$ in all these cases. Only few AS data-points are presented since this measurement imposes a stringent requirement: The density distribution along the sample has to be very smooth, so that the density in the source junction would be identical to the densities in both drain junctions. This implies that the maximal tunneling-rate appearing at $B = B^+$ will occur at the same magnetic field everywhere. The inset to Figure 4 shows that $G_{2T} = AS$ even when the density distribution is not perfectly smooth: In these cases the B^+ feature appearing in the asymmetry scan reflects the local density at the source junction, marked B_S^+, and the B^+ feature of the 2-terminal measurement reflects density in larger regions at the drains. The AS result is therefore taken at B_S^+ and should be compared to G_{2T} at the same field. This is done by super-imposing a data-point $AS(B_S^+)$ on a plot of $G_{2T}(B)$, taken at the same conditions. In order to present compiled data from different scans, where the height and width of the $G_{2T}(B)$ Lorentzian are different, we normalize each Lorentzian to unity height and width, and apply the same transformation to the respective $AS(B_S^+)$ data-point, verifying that $AS(B_S^+) = G_{2T}(B_S^+)$.

The compiled measurements presented in Figure 4 show that the result $AS = G_{2T}$ is robust: It holds for different samples, at different densities, and even when the sample has an uneven density-distribution. Returning now to Eq. 3, we have $(2f - 1) = g_c$, confirming that the fractionalization factor is $f = (g_c + 1)/2$, as theoretically predicted by

Luttinger theory[4] for an ideal momentum-conserving directional injector. To determine the value of f we need an independent evaluation of g_c. Following the method outlined in [21] we measure the tunneling conductance of the source junction as a function of both B and V_{SD}, allowing us to extract the spin and charge-mode dispersions. According to Luttinger liquid theory, for a Galilean invariant system, $g_c = v_F/v_c$. We thus obtain values of $0.4 < g_c < 0.5$, as observed in our previous work for the range of our observed densities implying that the fractionalization ratios are in the range of $0.7 < f < 0.75$.

In summary, we have measured an asymmetry in the electrical current obtained by injecting directional electrons into a quantum wire, and have found a direct relation between it and the separately measured two-terminal conductance. This relation can be explained by a simple model for an interacting single-mode wire, provided that each injected electron is fractionalized, with a forward-moving fraction $f = (g_c + 1)/2$, where g_c is the charge coupling constant that enters Luttinger liquid theory. This fraction is in fact the result predicted by Luttinger liquid theory for injection at an ideal momentum-conserving contact. The actual values of g_c, and thus of f, were determined from tunneling measurements as a function of source-drain voltage and magnetic field.
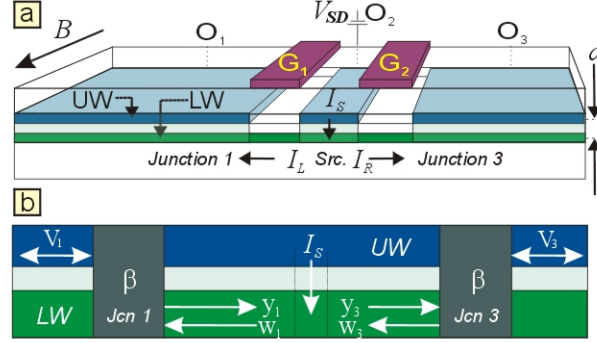
Figure 1: a, Cleaved-Edge-Overgrowth sample. Both wires (UW – blue; LW - green) form on the cleaved edge, facing the page. The UW is at the edge of a populated 2DEG (light blue) serving as a contact, through ohmic contacts O_1, O_2, O_3. 2-terminal geometry is realized by biasing gate G_1 to deplete the UW, so that transport takes place by tunneling into the LW and back via tunnel-junctions 1 and 3. The 3-terminal geometry is realized by depleting the UW using both gates $G_{1,2}$, which define a finite source junction. Contact O_2 is biased, and DC current to drains O_1, O_3 is measured. Magnetic field B applied perpendicular to the cleave plane allows momentum-control of tunneling.

b, Phenomenological model: Junctions 1 and 3 are characterized by parameter β. In junction 1, the chemical potential of the outgoing LW charge-mode y_1 depends on the incoming potential w_1 and the UW potential V_1. The same holds for junction 3. In the 3-terminal geometry current I_S is injected at the source. Note: $V_{1,3}$ are the UW electron-potentials at the junction, in equilibrium with the 2DEG.
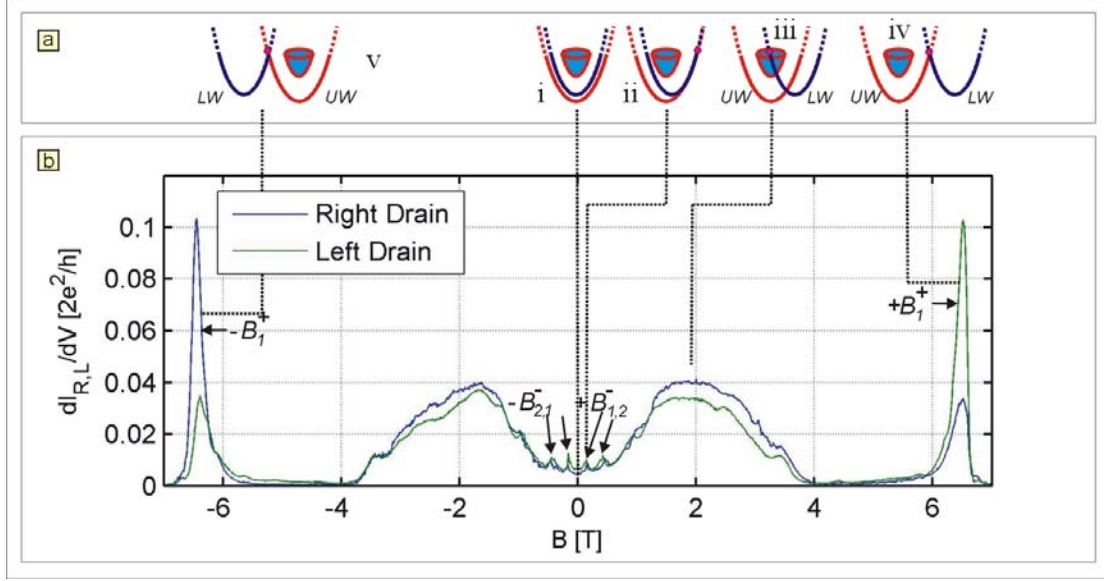
Figure 2: 3-Terminal asymmetry measurement. a, Annotations depicting the dispersion arrangement for each major feature. Blue (red) - single mode in the LW (UW). UW 2DEG is depicted by rotated dispersion. (i) $B = 0$; (ii) $B = B^-$; (iii) 2D-1D tunneling (iv) $B = +B^+$; (v) $B = -B^+$. The red dot represents the injected electrons. Note that since the UW density is larger than the LW density, at $B = B^-$ right movers are injected. At $B = B^+$ left movers are always injected. **b,** Differential conductance at the right and left drains is plotted vs. B. Current is detected whenever populated states in one wire overlap unpopulated states in the other. The wide features around $B = \pm 2T$ are associated with tunneling from the upper 2D to the LW. The sharp features at $B = \pm 6.5T = \pm B^+$ are associated with the overlap of counter-propagating 1D states in both wires. When $B = +B^+$, left-moving electrons are injected to the LW, and the majority of the current is detected at the left drain. At $B = -B^+$ the majority of the current is detected at the right. The right / left vs. $B^\pm$ symmetry attests to the geometrical symmetry of the right and left drains.
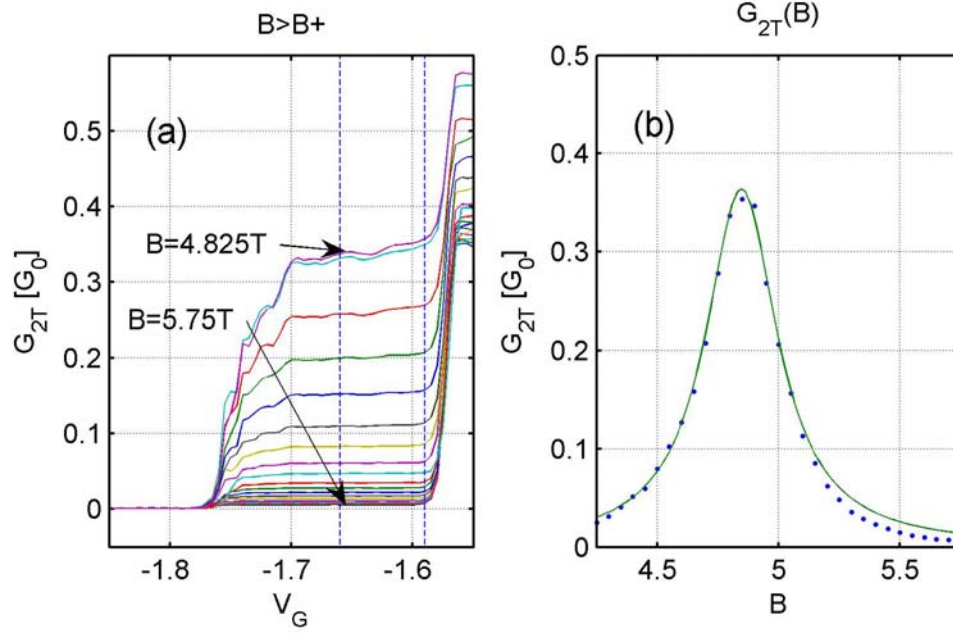
Figure 3: 2-terminal conductance scans. a, G_{2T} vs. V_G, for 4.825 T $< B <$ 5.75 T. The LW conductance step is defined between V_G =-1.58 V, where the last UW mode closes, and V_G=-1.76 V, where the LW closes. Coupling to the LW is done via junctions 1, 3 (Fig. 1). The height of the step increases as B approaches B^+. At each B, the data-point $G_{2T}(B)$ is defined as the maximal value in the range marked by the two vertical lines. **b,** G_{2T} vs. B, as extracted from (a). The solid line is a Lorentzian fit. $B < B^+$ scans are omitted from (a) for clarity.
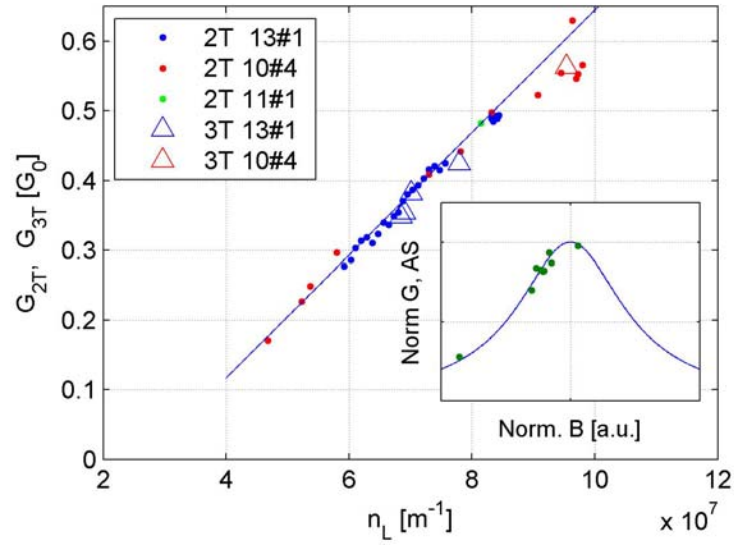
Figure 4: G_{2T} **(dots) and AS (triangles), plotted vs. LW density n_L for three different samples.** The line is a linear fit. Density control: Sample 13#1 – side-gate; 10#4, 11#1 – Illumination. *Inset*: AS vs. B_S^+ (dots); $G_{2T}(B)$ Lorentzian (line). In order to present compiled data from different densities, where Lorentzian width and height vary, we normalized each Lorentzian to unity width and height. AS vs. B_S^+ data-point is then subject to the same normalization (see text).

References

1. de-Picciotto, R. et al. Direct observation of a fractional charge. *Nature* **389**, 162-164 (1997).
2. Laughlin, R. B. Anomalous Quantum Hall Effect: An incompressible quantum fluid with fractionally charged excitations. *Phys. Rev. Lett.* **50**, 19395 (1982).
3. Saminadayar, L., Glattli, D. C., Jin, Y. & Etienne, B. Observation of the e/3 Fractionally Charged Laughlin Quasiparticle. *Phys. Rev. Lett.* **79**, 2526 (1997).
4. Pham, K.-V., Gabay, M. & Lederer, P. Fractional excitations in the Luttinger liquid. *Phys. Rev. B* **61**, 16397 (2000).
5. Safi, I. & Schulz, H. J. Transport in an inhomogeneous interacting one-dimensional system. *Phys. Rev. B* **52**, 17040 (1995).
6. Lorenz, T. et al. Evidence for spin-charge separation in quasi-one-dimensional organic conductors. **418**, 614 (2002).
7. Auslaender, O. M. et al. Spin-charge separation and localization in one dimension. *Science* **308**, 88-92 (2005).
8. Orgad, D. et al. Evidence of Electron Fractionalization from Photoemission Spectra in the High Temperature Superconductors. *Phys. Rev. Lett.* **86**, 4362 (2001).
9. Martin, J. et al. Localization of fractionally charged quasi-particles. *Science* **305**, 980 (2004).
10. Maslov, D. L. Transport through dirty Luttinger liquids connected to reservoirs. *Phys. Rev. B* **52**, 14368-14371 (1995).
11. Maslov, D. L. & Stone, M. Landauer conductance of Luttinger liquids with leads. *Phys. Rev. B* **52**, R5539 (1995).
12. Oreg, Y. & Finkel'stein, A. M. dc transport in quantum wires. *Phys. Rev. B* **54**, R14265 (1996).
13. Ponomarenko, V. V. Renormalization of the one-dimensional conductance in the Luttinger-liquid model. *Physical Review B* **52**, R8666 (1995).
14. Ponomarenko, V. V. & Nagaosa, N. Features of renormalization induced by interaction in one-dimensional transport. *Phys. Rev. B* **60**, 16865 (1999).
15. Lebedev, A. V., Crepieux, A. & Martin, T. Electron injection in a nanotube with leads: Finite-frequency noise correlations and anomalous charges. *Phys. Rev. B* **71**, 075416 (2005).
16. Dolcini, F., Trauzettel, B., Safi, I. & Grabert, H. Transport properties of single-channel quantum wires with an impurity: Influence of finite length and temperature on average current and noise. *Phys. Rev. B* **71**, 165309 (2005).
17. Trauzettel, B., Safi, I., Dolcini, F. & Grabert, H. Appearance of fractional charge in the noise of nonchiral Luttinger liquids. *Phys. Rev. Lett.* **92**, 226405 (2004).
18. Bena, C., Vishveshwara, S., Balents, L. & Fisher, M. P. A. Measuring fractional charge in carbon nanotubes. *J. Stat. Phys.* **103**, 429 (2001).

19. Imura, K.-I., Pham, K.-V., Lederer, P. & Piéchon, F. Conductance of one-dimensional quantum wires. *Phys. Rev. B* **66**, 035313 (2002).
20. Le Hur, K. Dephasing of microscopic interferences from electron fractionalization. *Phys Rev Lett* **95**, 076801 (2005).
21. Auslaender, O. M. et al. Tunneling spectroscopy of the elementary excitations in a one-dimensional wire. *Science* **295**, 825 (2002).
22. Steinberg, H. et al. Localization transition in a ballistic quantum wire. *Phys. Rev. B* **73**, 113307 (2006).
23. Yacoby, A. et al. Nonuniversal Conductance Quantization in Quantum Wires. *Phys. Rev. Lett.* **77**, 4612-4615 (1996).